# Quasi-2D Colloidal Semiconductor Nanoplatelets for Narrow Electroluminescence

*Zhuoying Chen,* Brice Nadal, Benoit Mahler, Hervé Aubin, and Benoit Dubertret*

**The first functional light-emitting diodes (LEDs) based on quasi 2D colloidal core/shell CdSe/CdZnS nanoplatelets (NPLs). The solution-processed hybrid devices are optimized with respect to their electroluminescent characteristics, first, by improving charge injection through exchanging the as-synthesized NPL long-chain ligands to shorter ones such as 3-mercaptopropionic acid, and second, by comparing different hole-transporting layers. NPL-LEDs exhibit a maximum luminance of 4499 cd $m^{-2}$ and external quantum efficiencies of 0.63%. In particular, over different applied voltages, systematically narrow electroluminescence of full width at half maximum (FWHM) in the range of 25–30 nm is observed to be independent from the choice of device configuration and NPL ligands. As spectrally narrow electroluminescence is highly attractive in terms of color purity in the context of LED applications, these results emphasize the unique potential of this new class of colloidal core/shell nanoplatelet in achieving bright and functional LEDs of superior color purity.**

## 1. Introduction

Colloidal nanocrystals have recently aroused extensive interest as luminophores for the realization of next-generation low-cost and high-efficiency light-emitting diodes (LEDs) for lighting and display applications.[1–11] Their potential in such applications originates from their low-cost synthesis, solution-processability, and their unique optical properties allowing spectrally narrow, bright and tunable emission from the whole visible spectrum to the near IR.[12] In the search for new colloidal nanocrystals displaying enhanced optical properties for light-emitting diodes (LED) applications, the question of morphology, *i.e.* whether quasi-spherical colloidal nanocrystal quantum dots should be the unique and best choice, remains to be explored. For colloidal quantum dots (QDs), strict control over the three dimensions on their surface chemistry, morphology and size are often necessary in order to obtain highly monodispersed nanocrystals allowing spectrally narrow electroluminescence, which is highly relevant in terms of color purity under the context of LED applications. Such strict 3D control requires extensive synthetic effort and may not be systematically achievable when it comes to scaled-up synthesis or when significant crystal growth after homogenous nucleation is needed, e.g., for large quantum dots of a specific emission. Indeed, up to now most colloidal LEDs based on spherical QDs, such as cadmium and zinc chalcogenide QDs for visible-emitting LEDs[1–3,7,9,13] and lead chalcogenide QDs for near-IR LEDs,[11] typically reported electroluminescence (EL) of full width half maximum (FWHM) larger than 30 nm, except for a few blue-emitting QD LEDs where relatively small QDs were employed.[7,9]

By comparison, studies of LEDs based on nanocrystals of other anisotropic shapes such as nanorods and nanoplatelets are rare, even though light-emitting devices built from epitaxially grown quantum wells are widely employed.[14] A major reason explaining the paradox resides in the fact that the synthetic protocols for atomically flat colloidal CdSe, CdS and CdTe quantum wells or nanoplatelets with thicknesses controlled at the atomic level have only been developed recently.[15,16] These nanoplatelets (NPLs), with a largely 2D structure, fall in the strong quantum confinement regime and exhibit thickness-tunable emission. They exhibit large exciton binding energy due to the combination of their two-dimensional character, large in-plane electron effective mass and relatively small dielectric constant,[17] and appear as the fastest colloidal fluorescent emitters (with nanosecond time-scale fluorescence lifetime at cryogenic temperature)[15,18] possibly due to a giant oscillator strength transition.[19] Due to their relatively larger crystal volume compared to QDs, NPLs can potentially exhibit less severe Coulomb blockade effects and allow more efficient charge injections without compromising quantum confinements. In terms of colloidal synthesis for spectrally narrow emitters, while strict controls over three-dimensions are necessary for QDs, NPLs require precise control only in their thickness where quantum confinement happens. As a result of their uniform thickness, core-only and core/shell NPLs typically exhibit extremely narrow solution photoluminescence (PL) of about 7 nm and 20 nm in FWHM respectively at room temperature,[15,16] which is highly desirable for color purity improvement under the context of LEDs. In this work, we demonstrate functional LEDs based on the recently synthesized[16] quasi-2D colloidal

Dr. Z. Chen, Dr. B. Nadal, Dr. B. Mahler,
Dr. H. Aubin, Dr. B. Dubertret
Laboratoire de Physique et d'Etude des Matériaux
ESPCI/CNRS/Université Pierre et Marie Curie
UMR 8213, 10 Rue Vauquelin, 75005, Paris, France
E-mail: zhuoying.chen@espci.fr

**DOI: 10.1002/adfm201301711**

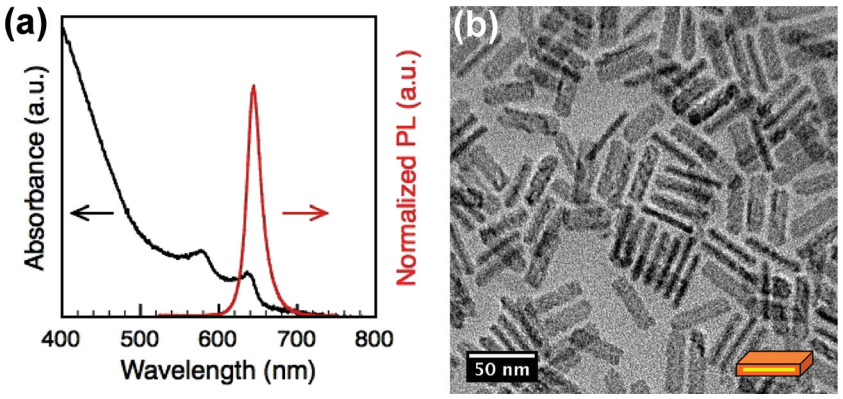


**Figure 1.** (a) Room-temperature absorbance and photoluminescence of core/shell CdSe/CdZnS NPL thin films. (b) Bright-field TEM image of the NPLs used in this study (inset in the lower right corner shows the schematic of a core/shell NPL).

core/shell CdSe/$Cd_{0.7}Zn_{0.3}S$ NPLs as the emissive material. 1.2 nm-thick CdSe NPL cores were passivated by a 2-nm-thick $Cd_{0.7}Zn_{0.3}S$ (below referred as CdZnS) shell. Such CdZnS shell was employed in order to achieve a regular shell morphologies and enhance the stability of luminescence properties of core-only NPLs.[16,20] Based on different device structures and NPL ligands, the device and electroluminescence characteristics of NPL-LEDs were optimized exhibiting a maximum luminance of 4499 cd/$m^2$ and external quantum efficiencies (EQE) of 0.63%. In particular, these NPL-LEDs allow extremely narrow electroluminescence over different applied voltages with a FWHM in the range of 25–30 nm.

## 2. Results and Discussion

Thin films of core/shell CdSe/CdZnS NPLs spin-coated from a cyclohexane solution exhibit a characteristic absorbance where the first two excitonic transitions correspond to the heavy-hole and light-hole transitions[15] (**Figure 1**a). From the onset of absorbance we estimate the optical band gaps of these NPLs thin films to be about 1.9 eV. At room temperature NPL films show red PL centered at about 646 nm with a FWHM of 21 nm. The dimensions of NPLs before and after shell growth were characterized by transmission electron microscopy (TEM). A typical TEM image of NPLs after shell growth is shown in Figure 1b where both NPLs lying flat on the substrate and NPL standing on their edges can be observed. TEM characterizations of core-only NPLs and high-resolution TEM characterizations of core/shell NPLs are shown in Figure S1 (Supporting Information) where both NPL core and the shell structures are clearly visible. In average, these core/shell NPLs exhibit a rather uniform lateral dimension of ~45 nm by 15 nm and a total thickness of ~5.2 nm.

The device structure chosen to realize electroluminescence from these core/shell NPLs is a hybrid structure (**Figure 2**a),

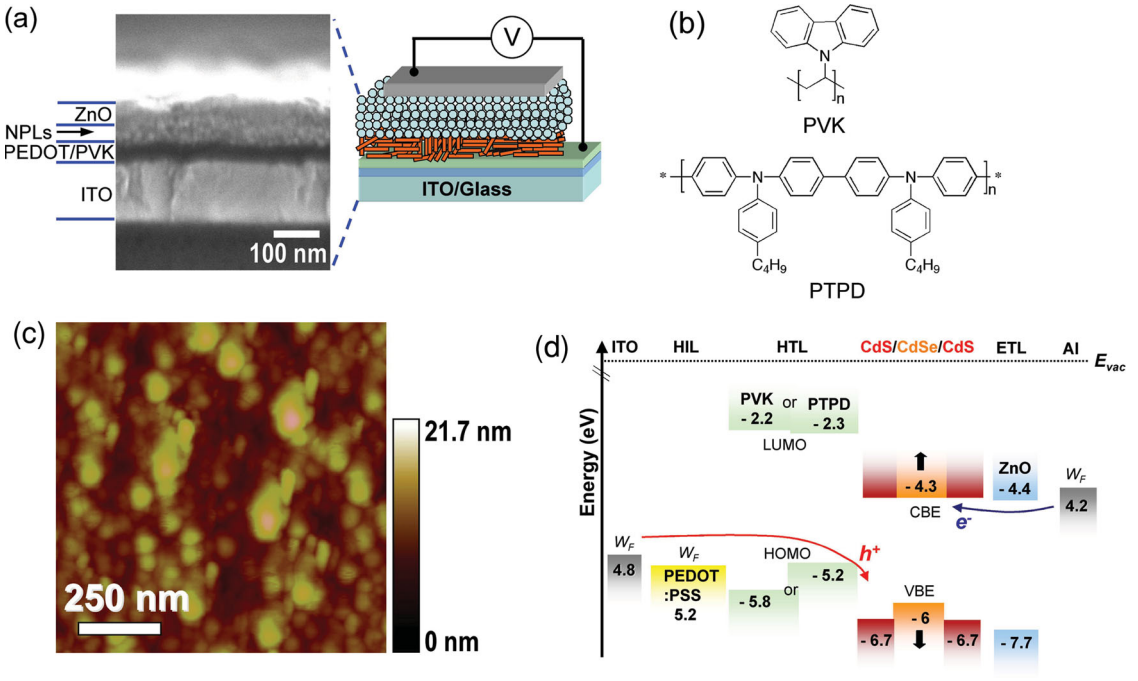


**Figure 2.** (a) Schematic representation (right) and cross-sectional SEM image (left) of a hybrid NPL-LED device (the Al top contact was not shown in the area where the SEM image was taken). (b) Molecular structures of the two hole-transporting polymers used in this study. (c) AFM height images of CdSe/CdZnS NPL thin films spun from cyclohexane. (d) Schematic energy-level diagram for the various layers used assuming vacuum level alignment (band bending and effects from the external electric field are not shown). The work functions ($W_F$) of ITO, PEDOT:PSS, Al, and the HOMO/LUMO of PVK and PTPD were taken from literature.[7,21–23] The conduction band edge (CBE) and valence band edge (VBE) values of CdSe and CdS were taken from bulk values.[36,37] The black arrows indicate the shift of band edges due to quantum confinement.

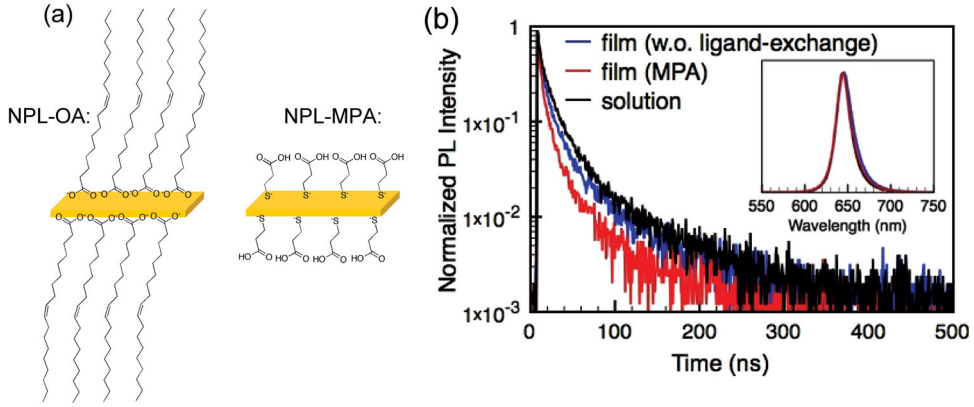


**Figure 3.** (a) Schematic representation of a NPL without ligand-exchange (with as-synthesized oleic acid as ligands, NPL-OA) and a NPL with ligands exchanged to MPA (NPL-MPA). (b) PL decay curves of diluted hexane solution (black lines) and thin films (blue and red lines) of CdSe/CdZnS NPLs. Blue and red lines are respectively PL decay curves from films without and with ligands exchanged to 3-mercaptopropionic acid (MPA). The inset of (b) shows the corresponding PL emission over wavelength. PL decay curves are collected at the PL peak emission energy of each sample.

where all layers were solution-processed except for the indium-tin oxide (ITO) anode and the aluminum cathode. With an emissive nanocrystal layer sandwiched between organic and inorganic metal-oxide layers that serve as both charge transport layers and optical spacers,[12] similar hybrid structures have been shown as a promising structure to achieve state-of-the-art colloidal QD-LED performance.[3,4,7–9,21] EL from such device structure is generally considered to originate from both direct charge injections and possibly energy transfer mechanisms.[12] As shown in the cross-sectional scanning electron microscopy (SEM) image and the schematic representation of a NPL-LED (Figure 2a), the core/shell NPL thin film layer (30–40 nm thick) are sandwiched between an inorganic electron transport layer (ETL, ~60 nm) of ZnO nanoparticles and a hole transport layer (HTL) made of semiconducting polymers of either poly(vinylcarbazole) (PVK, ~20–30 nm) or Poly(*N,N′*-bis(4-butylphenyl)-*N,N′*-bis(phenyl)benzidine (PTPD, ~30–40 nm) (Figure 2b). The middle NPLs layer was spin-coated at room temperature from their solutions with solvents in which PVK or PTPD do not dissolve[7,21] (fabrication and measurement details are described in the experimental section). Atomic force microscopy (AFM) topography images of NPL films spun from cyclohexane reveal irregular domains of clusters of NPLs with a typical surface roughness of 3–4 nm (Figure 2c). These layers are further sandwiched between an ITO anode, with its work function modified by a thin hole injection layer (HIL, ~20 nm) of PEDOT:PSS, and an aluminum cathode. According to the reported work function, the highest-occupied-molecular-orbital (HOMO) and lowest-unoccupied-molecular-orbital (LUMO) energy levels of each of these layers (Figure 2d),[7,21–23] we expect relatively efficient hole injection from the anode to the PTPD and efficient electron injection from the cathode to the ZnO layer, while some barrier exists to inject holes into the PVK. Once carriers are transported to the interface between the transport layer and the middle NPL layer, further electron injection from the ETL to the middle layer should be straightforward, while a higher energy barrier needs to be overcome to inject holes from PTPD into NPLs compared to the case of PVK. This hole-injection barrier is related to the lower-lying valence band edge of the core/shell nanocrystals (in particular for the wide-band-gap inorganic shell). In addition, the long-chain insulating surface ligands (i.e., oleic acid for as-synthesized NPLs) are expected to bring additional injection barriers.

To improve charge injection we experimented NPLs thin films with and without surface ligands exchanged to 3-mercaptopropionic acid (MPA) (**Figure 3**a) using a layer-by-layer spin-coating and exchange technique.[24] Exchanging the long-chain ligands to shorter ones, such as MPA or alkyldithiol, has been shown to improve significantly charge injection and transport.[25,26] We expect that the actual advantage of ligand-exchange on our device performance will depend on a compromise between charge injection enhancement and the possible decrease of PLQE due to surface modifications.[27] Due to the passivation of the inorganic shell employed here, nearly identical PL spectra, without observable trap-emission, were observed from NPL thin films before and after ligand-exchange with MPA (inset of Figure 3b). No obvious PL red shift was observed when comparing NPL solution and thin film PL owing to their uniform thickness. We performed PL decay measurements to estimate the decrease of PLQE NPL thin films upon film formation and upon ligand-exchange with reference to their dilute solution counterparts (Figure 3b). After the removal of excess ligands from their growth solution, core/shell CdSe/CdZnS NPL solution exhibit a PLQE of about 30%. The difference between the PL lifetime of solution and thin film samples is very small which suggests a minor (~10%) reduction of PLQE upon film formation. After ligand exchange to MPA, even though maintaining a nearly identical PL spectrum, NPL thin films exhibit a decreased PL lifetime from which we inferred about 40% decrease of PLQE associated with the surface ligand modification.

We then compared the use of NPLs with ligands exchanged to MPA (called NPL-MPA below), achieved through 3-times of layer-by-layer spin-coating and exchange process, and NPL films of equivalent total thickness (~30 nm) without ligand-exchange in a hybrid PVK/NPL(or NPL-MPA)/ZnO LED structure. Different thicknesses of the NPL emission layer were compared and the optimized thickness was found to be about 30 nm (Supporting Information, Figure S2). As shown in **Figure 4**a (black and red curves), while both PVK/NPL/ZnO and

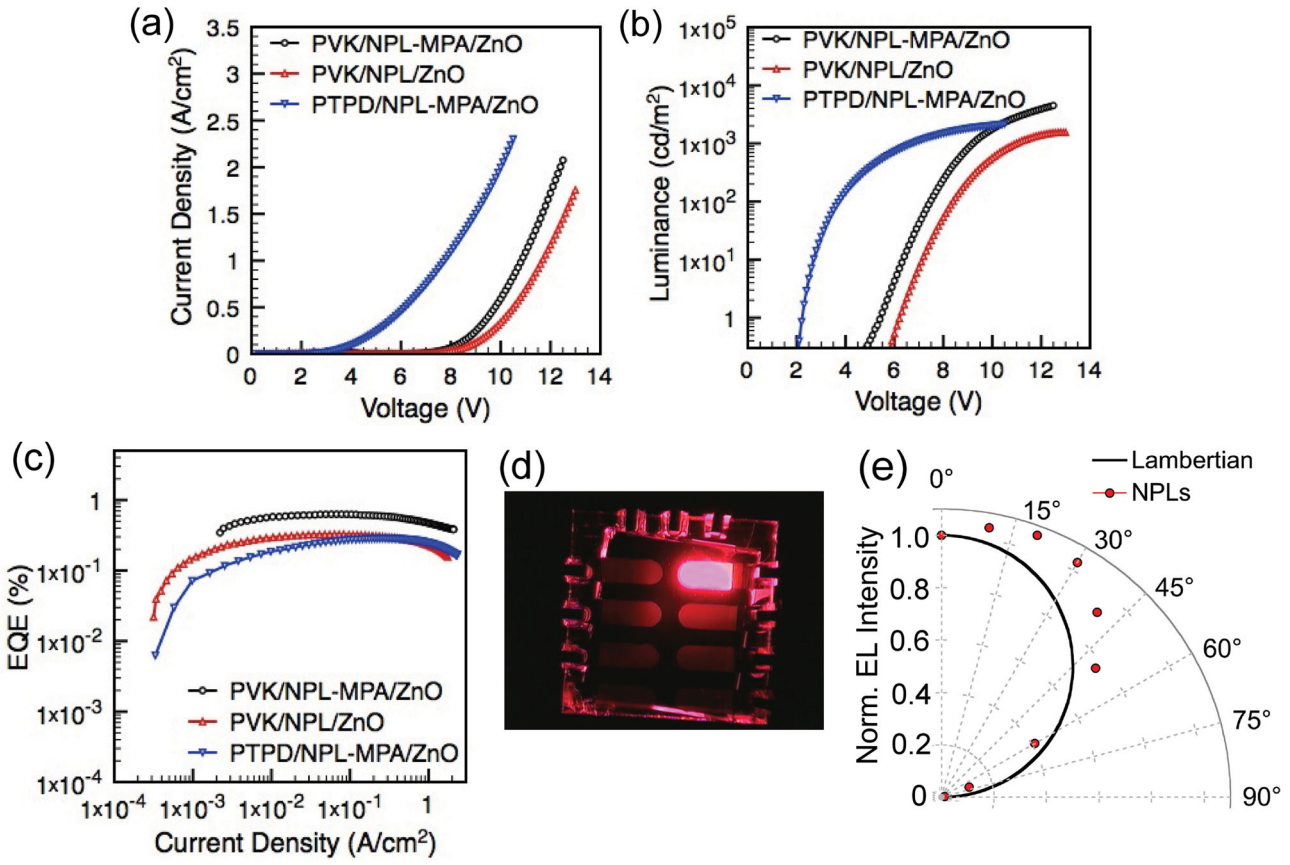


**Figure 4.** (a) Current density-voltage, (b) the corresponding luminance-voltage, and (c) EQE-current density characteristics of LEDs based on core/shell CdSe/CdZnS NPLs employing PVK/NPL-MPA/ZnO (black circles), PVK/NPL/ZnO (red triangles) and PTPD/NPL-MPA/ZnO (blue triangles) layers, sandwiched between ITO/PEDOT:PSS and Al. NPL-MPA refers to NPLs with ligands exchanged to MPA. (d) Photograph of a typical NPL-LED (with an emitting area of 4 $mm^2$) under an applied voltage of 10 V. (e) Normalized angular emission profiles of a representative NPL-LED measured on a rotation stage (with device edges masked). The dark line represents the Lambertian emission profile.

PVK/NPL-MPA/ZnO devices yield functional LEDs, upon turn-on PVK/NPL-MPA/ZnO devices exhibit an overall increase in both electric current densities and luminance with a slightly reduced EL turn-on voltage compared to unexchanged NPL-devices. This lead to an about 2-fold increase in the external quantum efficiency (EQE) of hybrid NPL-LEDs associated with ligand-exchange, reaching about 0.63% in EQE and a maximum brightness of 4499 cd $m^{-2}$ in PVK/NPL-MPA/ZnO devices (Figure 4). This enhanced device performance upon ligand-exchange suggests that in this case the resulting beneficial effect on charge injection can overweight the decrease of PLQE in the active NPL films. The angular dependence of electroluminescence from NPL-LEDs (with edges masked) deviates to some extent from the Lambertian emission pattern (Figure 4e), possibly due to either the anisotropic shape of the NPLs favoring a flat deposition on the substrate, or to the relatively low refractive index of the hole-transporting polymers compared to that of the inorganic layers (NPLs and ZnO) causing optical waveguiding.[28] Such a deviation has been taken into account when calculating the EQE of the devices in this study.

Employing the optimized NPL-MPA layer, the use of another semiconducting polymer PTPD, which typically exhibits higher hole drift mobilities (~$10^{-5}$ $cm^2$ $V^{-1}$ $s^{-1}$)[29] than PVK (drift mobilities ~$10^{-7}$–$10^{-6}$),[30] was then compared with PVK within the same polymer/NPL-MPA/ZnO device structure. As shown in Figure 4 (blue curves), PTPD/NPL-MPA/ZnO devices are also functional, exhibiting an attractive lower EL turn-on voltage of about 2 V. At such a small forward bias, while the efficient electron injection originates from the close alignment between the electron affinities of NPLs, ZnO, and the work function of aluminum, the efficient hole injection can be understood as a combination of the HOMO-work function alignment between PTPD and PEDOT:PSS and the possibility of an Auger-assisted hole injection process from PTPD to NPLs.[7] Despite the advantageous lower EL turn-on voltage compared to PVK/NPL-MPA/ZnO devices, PTPD/NPL-MPA/ZnO devices (Figure 4 black and blue curves) exhibit reduced luminance under the same current densities even though the overall electric current densities are increased. The resulting higher EQE in PVK/NPL-MPA/ZnO devices despites the lower mobility of PVK suggests that PTPD/NPL-MPA/ZnO devices are probably dominated by hole currents. The excess of holes in PTPD-devices can contribute to the resultant high electric current through either leakages into the sub-gap states of the ZnO

**Table 1.** Summary of the LED Characteristics based on Core/Shell CdSe/CdZnS NPLs.

| Active NPL Layer | PLQE[a] [%] | Device Structure[b] | Max. EQE [%] | | | | | |
|---|---|---|---|---|---|---|---|---|
| | | | $V_{on}$[c] [V] | $L_{max}$[d] [cd m$^{-2}$] | Peak | @ $10^3$ cd m$^{-2}$ | FWHM (nm) (@$V_{applied}$-$V_{on}$) | CIE index[e] ($x$,$y$) |
| NPL | ~30% | PVK/NPL/ZnO | ~5.9 | 1550 | 0.33 | 0.26 | 27 (@ 6.1 V) | (0.73, 0.29) |
| NPL-MPA | ~20% | PVK/NPL-MPA/ZnO | ~4.7 | 4499 | 0.63 | 0.59 | 26 (@ 6.3 V) | (0.73, 0.29) |
| | | PTPD/NPL-MPA/ZnO | ~2 | 2173 | 0.28 | 0.27 | 28 (@ 6 V) | (0.70, 0.29) |

[a]The PLQEs of nanocrystals without ligand exchange were measured in solution. The PLQEs of nanocrystals with ligands exchanged were estimated from non-exchanged samples and the decrease of PL lifetime upon ligand-exchange; [b]The multi-layers are further sandwiched between the ITP/PEDOT:PSS and Al; [c]$V_{on}$ is the applied voltage when the luminance is detected by a NIST-calibrated photodetector; [d]$L_{max}$ is the maximum detected luminance; [e]CIE index represents the Commission Internationale de l'Eclairage color coordinate.

or non-radiative recombination with the electrons in ZnO and thus, lowering the overall device EQE. Detailed device characteristics are summarized in **Table 1**.

Both PVK(or PTPD)/NPL-MPA/ZnO hybrid LEDs exhibit good rectification behavior (**Figure 5**a). On a double logarithmic plot, the current-voltage ($J$–$V$) characteristics of PTPD/NPL-MPA/ZnO devices exhibit roughly three regimes: an initial leakage or Ohmic conduction of residual charge inside the sample ($J \propto V$), followed by a trap-limited regime ($J \propto V^n$, $n > 2$) over a small voltage range, and finally approaching to a space-charge limited conduction ($J \propto V^n$, $n = 2$). By comparison, similar as previous reported hybrid QD LEDs,[4] the $J$–$V$ characteristics of PVK/NPL-MPA/ZnO devices demonstrated long-lasted trap-limited conduction after turn-on over the rest of the voltage range, suggesting the existence of hole traps provided by PVK together with trap sites from NPLs.[4,31] With the existence of more hole traps and a lower drift mobility compared to PTPD, PVK provides a reduced amount of hole current that results in a better bipolar current balance, higher luminance and EQE. On the other hand, the use of PTPD allows a lower turn-on voltage due to the more efficient hole injection and possibly, a reduced amount of hole traps.

Free from any parasitic emission from the polymer, ZnO or surface states of NPLs, our NPL-LEDs employing various hybrid structures [PVK (or PTPD)/(NPL or NPL-MPA)/ZnO] all exhibit clean emission originating *only* from the EL of the core/shell NPLs (**Figure 6**). No obvious differences in their EL spectra line shapes between NPL with or without ligand-exchange (Figure 6c) were observed. The slight variation of the EL peak under the same voltage between PVK and PTPD devices originates probably either from the different extent of charge injection (as PTPD devices turn on much earlier) or the slight variation in the total device thickness. EL spectra broadening and red shift (Figure 6a and b) were observed in NPL-LEDs with increasing applied voltage independently from the device and ligand types. From previous studies based on QDs we know that the EL broadening over applied voltages is related to the increased longitudinal optical phonon coupling,[32,33] while the EL red shift has been identified as a manifestation of quantum-confined Stark effect.[32–34] In an ensemble of QDs, the Stark shift is proportional to, where $\alpha$ is the polarizability.[32,33] The observed red shift of the EL peak position in our NPL-LEDs with reference to their PL peaks can indeed be fitted approximately with a quadratic function of the applied voltage (Figure 6d). From the stretch factor of the quadratic fit, a polarizability of about $1.7 \times 10^4$ Å$^3$ can be extracted respectively for NPLs. While the accuracy of the polarization extracted from such fits is limited by bias-stress effect and peak broadening, the polarizability value extracted from our NPL-LED is close to an order of magnitude smaller than the physical volume of the NPL core (~$6 \times 10^5$ Å$^3$). Such discrepancy may come from the strong geometric anisotropy of NPLs and from the fact that they may not all oriented perpendicularly to the field. Most importantly, despite the peak broadening effect from the applied electric field, it is

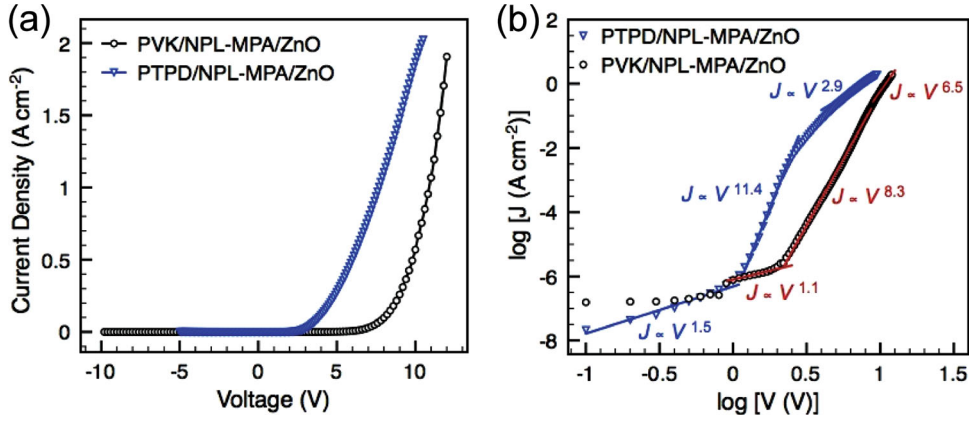


**Figure 5.** (a) Current-voltage characteristics showing both reverse and forward bias regimes indicating rectifying behaviour and (b) double logarithmic plot of the current-voltage characteristics of NPL-LEDs based employing PVK/NPL-MPA/ZnO (black circles) and PTPD/NPL-MPA/ZnO (blue triangles) as the active layers.

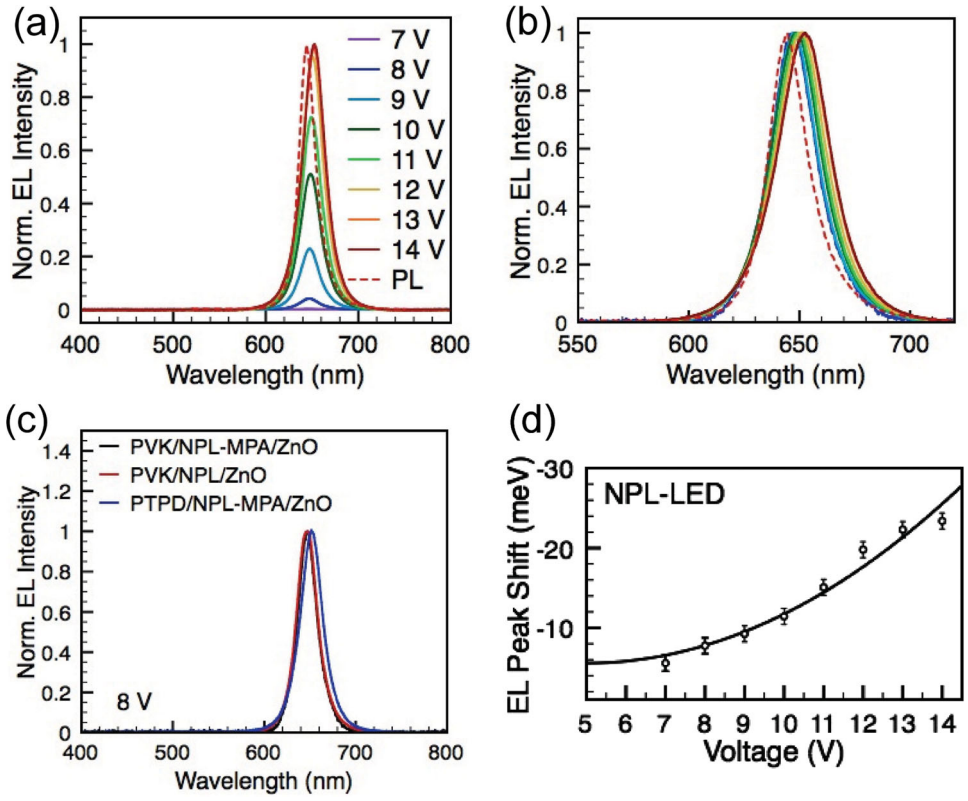


**Figure 6.** (a) Electroluminescence (EL) spectra of an optimized NPL-LED with the active layers based on the PVK/NPL-MPA/ZnO under different forward bias plotted together with the normalized PL spectra of the corresponding NPL films. The EL maximum associated with the highest applied voltage was normalized to 1. (b) The same EL spectra as (a) but with each spectrum maximum normalized to 1. (c) EL spectra of three NPL-LEDs, with their active layer respectively based on PVK/NPL-MPA/ZnO (black curve), PVK/NPL/ZnO (red curve), and PTPD/NPL-MPA/ZnO (blue curve), under 8 V of forward bias. (d) EL peak red shift over voltage (with reference to PL peak) extracted from the spectra shown in (a), fitted to a quadratic function of voltage (solid lines), and centered on the EL on-voltage observed from their *J-V-L* characteristics. Error bars represent the uncertainty of measurements from the spectrometer.

clear that NPL-LEDs exhibit a very narrower EL with a typical FWHM in the range of 25–30 nm over the different applied voltages (Figure 6 and Table 1). This significantly narrower EL from NPLs compared to the red EL achieved by currently reported QD-LEDs[1–3,7,9,13] promote NPLs as promising electroluminescent materials where the precise control on nanocrystal surface chemistry, morphology and size is only required in one dimension.

## 3. Conclusions

We have demonstrated the first functional LEDs based on quasi-2D colloidal core/shell CdSe/CdZnS nanoplatelets. With a solution-processed hybrid device structure where colloidal NPLs are sandwiched between a hole-transporting polymer and an electron-transporting ZnO nanoparticle layer, we optimized the device and electroluminescence characteristics through applying different hole-transporting polymers as well as exploring the strategy of exchanging the as-synthesized NPL long-chain ligands to shorter ones such as MPA. These NPL-based LEDs exhibit high external quantum efficiencies reaching 0.63% together with a very narrow EL of FWHM in the range of 25–30 nm, depending on the applied voltages. The present results indicate that these recently-developed colloidal core/shell nanoplatelets provide a new class of material systems with unique potential in achieving superior color purity for light-emitting applications.

## 4. Experimental Section

*Synthesis of CdSe NPL Cores*: 90 mL of 1-Octadecene (ODE), 480 mg of cadmium acetate dihydrate ($Cd(OAc)_2(H2O)_2$), and 1.18 g of oleic acid (OA) were introduced into a 250 mL three-neck flask. The mixture was degassed under vacuum and magnetic stirring at 110 °C during 90 min. After filling the flask with argon, 72 mg of elemental Se powder dissolved in 2 mL of ODE was swiftly injected in the hot mixture and the temperature was set to 240 °C. When the temperature reached 205 °C, 240 mg of $Cd(OAc)_2(H_2O)_2$ was introduced in the reaction mixture and the reaction was allowed to proceed for 15 min at 240 °C. The mixture was then cooled down to room temperature and 10 mL of OA was added, inducing the aggregation of the platelets. The mixture was centrifuged for 10 min at 5000 rpm, the supernatant was discarded, and the precipitated NPLs were suspended in hexane. The NPLs were then precipitated one more time with ethanol and suspended in 10 mL of hexane.

*Synthesis of CdZnS Shell on CdSe NPL Cores*: CdZnS shell was prepared following a previously published method.[35] Briefly, 500 µL of CdSe core nanoplatelets in hexane was diluted in 4 mL chloroform. Then 100 mg of thioacetamide (TAA) and 1 mL of octylamine were added in the flask

and the mixture was sonicated until the complete dissolution of the TAA (about 5 min). The color of the solution changed from yellow to orange during this time. 350 µL of a solution of $Cd(NO_3)_2$ (0.2 M in ethanol) and 150 µL of a solution of $Zn(NO_3)_2$ (0.2 M in ethanol) are then added to the flask. The reaction was allowed to proceed for 24 h at room temperature. After synthesis, the core/shell platelets were isolated from the secondary nucleation by precipitation with a few drops of ethanol and suspended in 5 mL chloroform. To improve the stabilization and the quantum yield of the core/shell NPLs, 100 µL of $Zn(NO_3)_2$ solution (0.2 M in ethanol) is added to the NPLs solution. They aggregate steadily and are re-suspended by adding 200 µL of OA.

*Synthesis of ZnO Nanoparticles*: ZnO nanoparticles were synthesized following a previously published method.[7] Briefly, in two separated containers we dissolved tetramethylammonium hydroxide (TMAH) in 30 mL of ethanol (0.55 M) and zinc acetate dihydrate into 90 mL of dimethyl sulfoxide (DMSO) (0.1 M). The TMAH solution was then mixed and stirred with the zinc acetate solution for 1 hour in ambient conditions at room temperature. After 1 h we precipitated ZnO nanoparticles from their growth solution by adding ethyl acetate. The precipitate was collected and re-dispersed in ethanol.

*Device Fabrication and Characterizations*: All solvents and polymers used in device fabrications were used as purchased without further purification. As-synthesized NPLs were precipitated from their growth solution using ethanol and then redispersed in hexane. This NPL-hexane solution was further purified by precipitation and centrifugation after adding a mixture of methanol and butanol. The precipitates were finally redispersed in anhydrous cyclohexane or toluene. Indium-tin oxide (ITO) substrates were first cleaned in an ultrasonic water bath containing 10% NaOH followed by a de-ionized water-rinsing step. They were further sonicated sequentially in a bath of de-ionized water, acetone, and finally isopropanol before drying with a nitrogen flow. A layer of PEDOT:PSS (Baytron P VP AI 4083) was then spin-coated on top followed by annealing at 230 °C under nitrogen or argon for 30 min. Poly(vinylcarbazole) (PVK, $M_w$~ 120 000) and poly(*N,N'*-bis(4-butylphenyl)-*N,N'*-bis(phenyl)benzidine (PTPD, $M_w$~ 10 000–70 000) were purchased respectively from Aldrich and American Dye Source Inc. Inside an argon-filled glovebox, we dissolved PVK and PTPD respectively in anhydrous 1,2-dichlorobenzene (12.5 mg/mL) and chlorobenzene (10 mg/mL) with subsequent filtering by a PTFE filter (0.45-micrometer pore size). PVK and PTPD layers were then deposited onto ITO/PEDOT:PSS substrates by spin-coating followed by annealing at 180 °C for 60 minutes (PVK) or at 120 °C for 30 min (PTPD). As PVK has little solubility in cyclohexane at room temperature,[21] cyclohexane solution of NPLs was used to deposit the active emission layer by spin-coating on top, while for similar reasons[7] toluene solution of NPLs was used to deposit on top of PTPD. For ligand-exchanged NPL-LEDs, after spin-coating a sub-layer of NPLs, we dipped the sample into a solution of acetonitrile containing 10% 3-mercaptopropionic acid (MPA) for 30s followed by a rinse of clean acetonitrile and drying under an argon flow. We repeated this layer-by-layer spin-coating[24] multiple times until a desired film thickness was reached. Typically, for a 30-nm-thick NPL layer, 3 layer-by-layer coatings were used. The ZnO nanoparticle layer (thickness controlled to be about 50–60 nm) was then further spin-coated on top from ethanol solutions followed by annealing at 145 °C for 30 min. An 100-nm-thick aluminum was then thermally evaporated in vacuum ($<4\times10^{-6}$ mbar) through a shadow mask onto the ZnO nanoparticle layer as the cathode. All devices were encapsulated under inert conditions before testing in air.

The shell thicknesses of core/shell NPLs were determined by TEM characterizations (JEOL 2010, 200 kV) before and after shell growth. SEM characterizations were performed with a FEI Magellan 400 system with a standard field emission gun source. UV-Visible absorption spectra were measured in air using a Varian Cary 5E UV-visible-NIR spectrometer. Photoluminescence (PL) and PL decay measurements were carried out at room temperature at ambient pressure for solution samples or under vacuum ($<10^{-5}$ mbar) in a cryostat for thin film samples by an Edinburgh Instruments spectrofluorometer. Samples were excited by a pulsed laser (wavelength = 376.8 nm, pulse width = 68.7 ps). All film thicknesses were measured using a profilometer (Veeco Dektak). AFM images were obtained using a Digital Instruments Nanoscope III AFM in tapping mode. The current-voltage-luminance (*J-V-L*) characterizations of LEDs were performed in air with a Keithley 4200-SCS Semiconductor Characterization System and a Low Noise Current Preamplifier (Stanford Research Systems SR570). A NIST-calibrated Si photodetector is placed in the forward direction with the luminance output calculated after correcting the derivation of the angular emission profile from a standard Lambertian emission. During *J-V-L* measurements device edges were masked by black tapes to minimize the contribution of edge-emitting light in the measured EQE. Angular Emission profiles were measured by placing devices on a rotation stage (also with device edges masked). EL spectra were recorded with a multimode optical fiber placed in the forward emission direction and attached to an Ocean Optics HR4000 spectrometer.

## Supporting Information

Supporting Information is available from the Wiley Online Library or from the author.

## Acknowledgements

Z. Chen acknowledges partial support from the project of ANR-2011-JS09–004–01-PvCoNano. Z. Chen is grateful to M. D. Tessier and T. Pons for helpful discussions.

Received: May 20, 2013
Published online: July 16, 2013

[1] Q. Sun, Y. A. Wang, L. S. Li, D. Wang, T. Zhu, J. Xu, C. Yang, Y. Li, *Nature Photonics* **2007**, *1*, 717.
[2] J. M. Caruge, J. E. Halpert, V. Wood, V. Bulovic, M. G. Bawendi, *Nature Photonics* **2008**, *2*, 247.
[3] P. O. Anikeeva, J. E. Halpert, M. G. Bawendi, V. Bulovic, *Nano Lett.* **2009**, *9*, 2532.
[4] K.-S. Cho, E. K. Lee, W.-J. Joo, E. Jang, T.-H. Kim, S. J. Lee, S.-J. Kwon, J. Y. Han, B.-K. Kim, B. L. Choi, J. M. Kim, *Nature Photonics* **2009**, *3*, 341.
[5] W. K. Bae, J. Kwak, J. Lim, D. Lee, M. K. Nam, K. Char, C. Lee, S. Lee, *Nano Lett.* **2010**, *10*, 2368.
[6] T.-H. Kim, K.-S. Cho, E. K. Lee, S. J. Lee, J. Chae, J. W. Kim, D. H. Kim, J.-Y. Kwon, G. Amaratunga, S. Y. Lee, B. L. Choi, Y. Kuk, J. M. Kim, K. Kim, *Nature Photonics* **2011**, *5*, 176.
[7] L. Qian, Y. Zheng, J. Xue, P. H. Holloway, *Nature Photonics* **2011**, *5*, 543.
[8] V. Wood, M. J. Panzer, D. Bozyigit, Y. Shirasaki, I. Rousseau, S. Geyer, M. G. Bawendi, V. Bulovic, *Nano Lett.* **2011**, *11*, 2927.
[9] J. Kwak, W. K. Bae, D. Lee, I. Park, J. Lim, M. Park, H. Cho, H. Woo, D. Y. Yoon, K. Char, S. Lee, C. Lee, *Nano Lett.* **2012**, *12*, 2362.
[10] B. N. Pal, Y. Ghosh, S. Brovelli, R. Laocharoensuk, V. I. Klimov, J. A. Hollingsworth, H. Htoon, *Nano Lett.* **2012**, *12*, 331.
[11] L. Sun, J. J. Choi, D. Stachnik, A. C. Bartnik, B.-R. Hyun, G. G. Malliaras, T. Hanrath, F. W. Wise, *Nature Nanotechnol.* **2012**, *7*, 369.
[12] Y. Shirasaki, G. J. Supran, M. G. Bawendi, V. Bulovi , *Nature Photonics* **2012**, *7*, 13.
[13] K. W. Song, R. Costi, V. Bulovic, *Adv. Mater.* **2013**, *25*, 1420.
[14] S. Nakamura, T. Mukai, M. Senoh, *Appl. Phys. Lett.* **1994**, *64*, 1687.
[15] S. Ithurria, M. D. Tessier, B. Mahler, R. P. S. M. Lobo, B. Dubertret, A. L. Efros, *Nat. Mater.* **2011**, *10*, 936.

[16] B. Mahler, B. Nadal, C. Bouet, G. Patriache, B. Dubertret, *J. Am. Chem. Soc.* **2012**, *134*, 18591.
[17] R. Benchamekh, J. Even, J.-M. Jancu, M. Nestoklon, S. Ithurria, B. Dubertret, P. Voisin, 20th Int. Symp. "Nanostructures: Physics and Technology", Nizhny NNovgorod, Russia, June 24–30, **2012**.
[18] M. D. Tessier, C. Javaux, I. Maksimovic, V. Loriette, B. Dubertret, *ACS Nano* **2012**, *6*, 6751.
[19] E. I. Rashba, G. E. Gurgenishvili, *Sov. Phys. Solid State* **1962**, *4*, 759.
[20] D. V. Talapin, I. Mekis, S. Götzinger, A. Kornowski, O. Benson, H. Weller, *The Journal of Physical Chemistry B* **2004**, *108*, 18826.
[21] J. W. Stouwdam, R. A. J. Janssen, *Journal of Materials Chemistry* **2008**, *18*, 1889.
[22] T. M. Brown, J. S. Kim, R. H. Friend, F. Cacialli, R. Daik, *Appl. Phys. Lett.* **1999**, *75*, 1679.
[23] R. Bittner, K. Meerholz, in *Photorefractive Materials and Their Applications 2* (Eds: P. Günter, J. P. Huignard), Springer, New York **2007**.
[24] A. G. Pattantyus-Abraham, I. J. Kramer, A. R. Barkhouse, X. Wang, G. Konstantatos, R. Debnath, L. Levina, I. Raabe, M. K. Nazeeruddin, M. Grätzel, E. H. Sargent, *ACS Nano* **2010**, *4*, 3374.
[25] R. S. Dibbell, D. F. Watson, *J. Phys. Chem. C* **2009**, *113*, 3139.
[26] K. S. Jeong, J. Tang, H. Liu, J. Kim, A. W. Schaefer, K. Kemp, L. Levina, X. Wang, S. Hoogland, R. Debnath, L. Brzozowski, E. H. Sargent, J. B. Asbury, *ACS Nano* **2012**, *6*, 89.
[27] D. R. Baker, P. V. Kamat, *Langmuir* **2010**, *26*, 11272.
[28] D. Kabra, M. H. Song, B. Wenger, R. H. Friend, H. J. Snaith, *Adv. Mater.* **2008**, *20*, 3447.
[29] C. Takahashi, S. Moriya, N. Fugono, *Synthetic Metals* **2002**, *129*, 123.
[30] J.-Y. Kim, M. Kim, J.-H. Choi, *Synthetic Metals* **2003**, *139*, 565.
[31] R. A. M. Hikmet, D. V. Talapin, H. Weller, *J. Appl. Phys.* **2003**, *93*, 3509.
[32] S. A. Empedocles, M. G. Bawendi, *Science* **1997**, *278*, 2114.
[33] V. Wood, M. J. Panzer, J. M. Caruge, J. E. Halpert, M. G. Bawendi, V. Bulovic, *Nano Lett.* **2010**, *10*, 24.
[34] J. Zhao, J. A. Bardecker, A. M. Munro, M. S. Liu, Y. Niu, I. K. Ding, J. Luo, B. Chen, A. K. Y. Jen, D. S. Ginger, *Nano Lett.* **2006**, *6*, 463.
[35] B. Mahler, P. Spinicelli, S. Buil, X. Quelin, J. P. Hermier, B. Dubertret, *Nat. Mater.* **2008**, *7*, 659.
[36] T. C. Chiang, F. J. Himpsel, *Landolt-Börnstein - Group III Condensed Matter*, Vol. 23a, Springer, Berlin **1989**.
[37] A. L. Efros, M. Rosen, *Annu. Rev. Mater. Sci.* **2000**, *30*, 475.